sensors

MDPI

Article

A New Method for the Measurement of the Diffusion Coefficient of Adsorbed Vapors in Thin Zeolite Films, Based on Magnetoelastic Sensors

Dimitris Kouzoudis [1,*], Theodoros Baimpos [2] and Georgios Samourgkanidis [1]

[1] Department of Chemical Engineering, University of Patras, GR 26504 Patras, Greece; g.samourgkanidis@gmail.com
[2] National Observatory of Athens, Lofos Koufou, P. Pendeli, GR-15236 Athens, Greece; t.baimpos@noa.gr
* Correspondence: kouzoudi@upatras.gr; Tel.: +30-2610-996880

Received: 21 May 2020; Accepted: 5 June 2020; Published: 7 June 2020

Abstract: In the current work an experimental method is used in order to calculate the diffusivity D (diffusion coefficient) of various vapors in thin zeolite films. The method is based on adsorption data from magnetoelastic sensors on top of which a zeolite layer was synthesized, and the diffusivity is extracted by fitting the data to Fick's laws of diffusion. In particular, the method is demonstrated for two volatile organic compound (VOC) vapors on two different zeolites, the p-Xylene adsorption in Faujasite type zeolite with $D = 1.89 \times 10^{-13}$ m^2/s at 120 °C and the propene adsorption in Linde Type A type zeolite with $D = 5.9 \times 10^{-14}$ m^2/s at 80 °C, two diffusion coefficients which are extracted experimentally for first time. Our results are within the order of magnitude of other VOC/zeolite values reported in literature.

Keywords: magnetoelastic; sensors; diffusion coefficient; zeolite; FAU; LTA

1. Introduction

Magnetoelastic sensors are an excellent tool for adsorption studies in thin films as their signal is sensitive to mass loads [1–6]. As it is shown in Figure 1, the voltage signal of a thin magnetoelastic strip, when excited along its long axis, exhibits resonance at a specific resonance frequency f_R. In general, it can be proven that a rectangular thin ribbon with length L of any material with density ρ, Young modulus E, and Poisson's ratio ν, resonates mechanically [7] at a frequency:

$$f_R = \frac{1}{2L}\sqrt{\frac{E}{\rho(1-\nu^2)}} \quad (1)$$

Typically, the magnetoelastic adsorption sensors are composed of two layers, one with the magnetoelastic material which acts as the sensing layer, and one with a chemically active material which selectively adsorbs the desired species. The adsorbed mass alters the density ρ in Equation (1) (because in an adsorption process the sensor mass changes but its volume remains the same) and the resonance frequency shifts toward lower values, assuming that the adsorption does not affect E (there are some exceptions with absorption-induced stresses that alter this assumption which are discussed later in the text). Thus, a proper calibration with known mass loads, can turn the resonating layers into microbalance sensors [1–4]. Our group has used successfully zeolite films as the chemically active layers, on top of magnetoelastic materials of type "Metglas", in order to detect a number of different gasses and analytes [5,6].

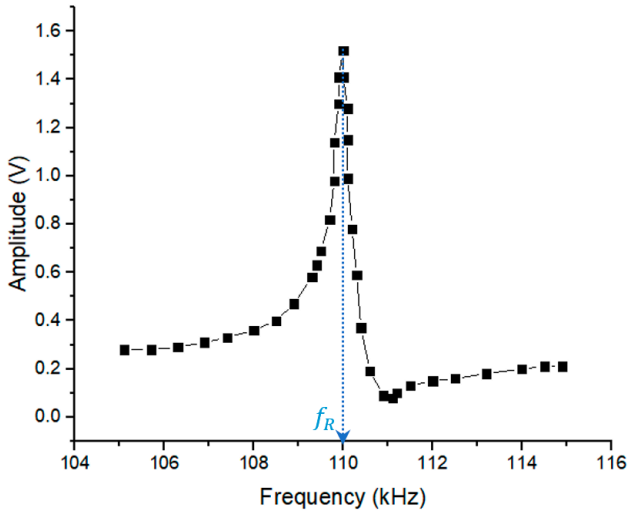

Figure 1. Standard voltage-frequency signal of a magnetoelastic sensor where the resonance peak is clearly seen.

On the other hand, volatile organic compounds (VOC) are considered hazardous in general and thus their detection and filtration are deemed necessary. Concerning the detection, a number of different detection techniques have been proposed in the past [6,8–14]. As for filtration, zeolites have played an active role towards this direction, due to their microporous structure, which allows for the trapping and the subsequent removal of VOC from certain atmospheres or other contaminated substances [15–18]. There are cases though, where removal of VOC by catalytic conversion has been successfully performed [19–21].

Of great importance in these applications, is the dynamics of the adsorption of VOC in the zeolite crystals which is basically the diffusion process. When it comes to diffusion, Fick's two laws come to mind, which can be summarized in the following differential equation,

$$\frac{\partial c}{\partial t} = D\frac{\partial^2 c}{\partial x^2} \tag{2}$$

which governs the diffusion process in one dimension. Here c is the concentration of the adsorbed VOC molecules (mass per distance) and D their diffusion coefficient in the zeolite film. A little discussion about the validity of the above equation should be given here. According to [22], Fick's laws appear to be valid only for homogeneous systems which is not the case for zeolite crystals when viewed at atomic scale, but they can be considered practically homogeneous when a large space scale is considered. In our case, our zeolite films had thicknesses of the order of micron-meters and the diffusion took place over this distance so we can safely assume that we are on the large scale side. Additionally, our films were not single crystals but were composed of a large number of single crystals (see SEM micrographs in [23]) which means that every physical property of the film has the meaning of an averaged quantity over all possible directions, thus uniformity can be safely assumed. Under these considerations, we can accept Fick's laws as valid laws to describe diffusion phenomena in our zeolite films.

Another point that needs to be considered is the fact that Equation (2) is valid for the case where only one species is diffusing through a solid material. When two or more species are present, the species do not act independently of each other but the diffusion of one affects the diffusion of the other species [24]. In such a case, the more general Maxwell–Stefan equations need to be used (see Equation (2) in [24]) and Equation (2) above is a special case of these equations when only one species is present. In our case, a binary mixture of gases was used with one being the VOC vapor. However, as the VOC are strongly adsorbed in the zeolite crystal and we are particularly interested on their diffusion dynamics, we can approximately use Equation (2) keeping in mind that the Maxwell–Stefan equations lead only to small corrections to the concentration profiles predicted by Equation (2).

The main purpose of the current work is to use our VOC sensing data which were recorded by magnetoelastic/zeolite strips, in order to extract the diffusion coefficient D in Equation (2) of the VOC in the zeolite crystal. The usefulness of the current method is that (a) there are not so many available VOC-zeolite data for D, (b) when available, there is a noticeable deviation among different authors, and (c) there is a variety of measuring techniques, some of which are not so easy to use and not so direct to interpret. Table 1 below gives a short review of diffusion coefficients D found by different authors for a number of VOC-zeolite combinations.

Table 1. Different diffusion coefficients for gas/zeolite pairs reported in the literature.

VOC	Zeolite Type	D (10^{-12} m^2/s)	Temperature (°C)	Reference
p-Xylene	ZSM-5	0.13	300	[25]
Benzene	ZSM-5	0.025	65	[26]
Benzene	ZSM-5	0.05	142	[27]
ethylbenzene	ZSM-5	0.049	142	[27]
i-Butane	ZSM-5	1	60	[28]
n-Butane	ZSM-5	0.8	200	[29]
n-Hexane	ZSM-5	0.46	200	[29]
2-Methylpentane	MFI	1	130	[30]
n-Hexane	MFI	45	130	[30]
methanol	NaX	10	100	[27]
Benzene	NaX	12	-	[27]
Benzene	NaX	12	195	[31]
propylene	NaY	1500	-	[32]
p-Xylene	NaY	0.18	25	[33]
Propene	5A	1.1–1.6	200	[29]
n-Butane	5A	0.5–0.7	200	[29]
n-Octane	USY	1100	25	[22]
n-Butane	Modernite	24,000	60	[28]
n-Hexane	Pt/HMOR	0.1	250	[34]

2. Materials and Methods

Figure 2 shows the experimental part that was used for the recording of the VOC adsorption data by magnetoelastic sensors. Our sensors were composed of two layers, one of which was of zeolite type, either Faujasite (FAU) or Linde Type A (LTA) (for more synthesis details and methods, please see [8]) of a few tens of microns thick, and another 30 μm thick layer composed of magnetoelastic material 2826 MBA, which is an amorphous metal with average stoichiometry $Fe_{40}Ni_{38}Mo_4B_{18}$. The sensor thickness and width were 2 and 0.4 cm correspondingly. The sensor was placed inside the glass-cell shown in Figure 2 and an excitation coil and a detection coil were wound around the cell. These coils were driven and interrogated by a special resonator which basically resonates the sensor and records its natural frequency on a personal computer. Before allowing any VOC atmosphere in the glass cell, the sensor was left overnight under the flow of dry synthetic air (referred to simply as "air" from now on) at a temperature of 120 or 80 °C (depending on the VOC, see adsorption experiments below) in order to clear its pores of unwanted components such as humidity. Following this clean-up procedure, a number of resonance data were recorded for a total period of 4 h with the same dry air flow and temperature. The results are shown in Figure 3. This experiment proves, as expected, that under a stable atmosphere the resonance frequency f of the laminate remains constant with a mean value of 102.88 kHz and a fluctuation of about ±0.05 kHz, thus providing us with an indication of the accuracy of the set-up. Going back to Figure 2, which was used for the VOC measurements, a saturator was used to create saturated VOC vapor when the VOC was in the liquid phase at normal conditions. As the figure shows, air was allowed to flow through the saturator which contained the liquid VOC. Parallel to that flow, was a dry flow of air and the two flows were mixed in a given ratio in order to create the desired VOC concentration inside the glass cell. The saturator was replaced by a VOC gas cylinder for certain VOC that exist in the gas phase at normal conditions. Two different VOC were

tested in the current work by two different sensors: (a) p-Xylene with a sensor with a FAU zeolite, and (b) propene with a sensor with an LTA zeolite. These combinations were chosen because these zeolites show selectivity on these two particular VOC.

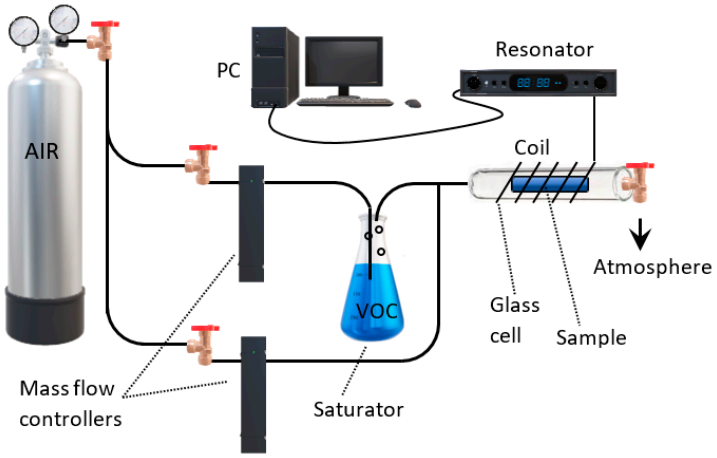

Figure 2. Experimental set-up for the detection of volatile organic compounds (VOC).

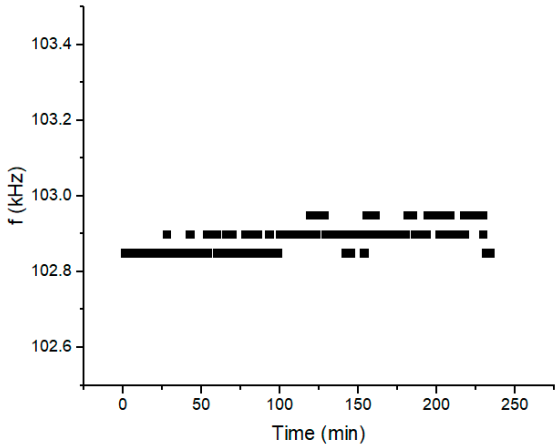

Figure 3. Measurement of the sensor resonance frequency for a period of 4 h under the presence of plain air, to check for the sensor stability.

3. Results

3.1. Case (a) p-Xylene/FAU

In this case, the VOC chosen was p-Xylene and the zeolite layer on the sensor was of FAU type and the adsorption measurements at 120 °C were as shown in Figure 4. These measurements are not new, but they were first presented in one of the author's PhD work [35]. In order to check the zeolite adsorption response, the sensor atmosphere was allowed to alternate between dry-air and VOC of various concentrations in ppm (parts per million with respect to clear air), and several resonance data were recorded in fixed time intervals. The plot shows the corresponding resonance frequencies f versus time. As it was mentioned in the introduction, f depends inversely on mass loads and so it drops when the VOC is introduced in the glass cell, after this was filled with clear air (since p-Xylene is heavier than air). It should be mentioned at this point, that at certain adsorption experiments, there was another important parameter, besides the mass load, that needed to be taken into consideration. This parameter was the development of internal adsorption-stresses on the zeolite film, which were capable of rising f during adsorption, thus contradicting our initial assumptions of a decreasing frequency

with mass load. However, in the data of Figure 4, such a behavior was not observed and so we were confident that the measured resonance frequency was entirely due to mass loads.

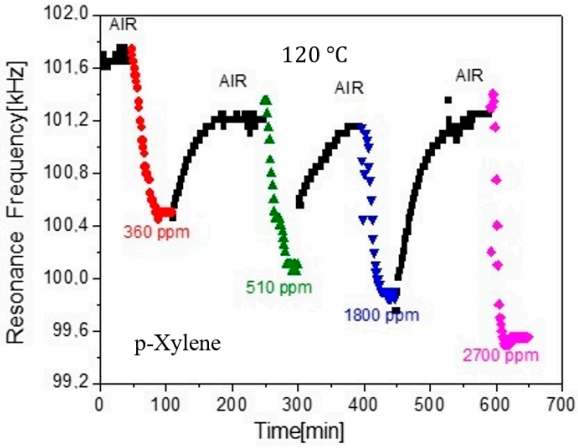

Figure 4. Data from PhD work [35], which corresponds to different p-Xylene concentrations on a Metglas/Faujasite (FAU) sensor.

3.2. Case (b) Propene/LTA

In this case, the VOC chosen was propene (C_3H_6) and the zeolite layer on the sensor was of LTA type and the adsorption measurements at 80 °C were as shown in Figure 5. As in Case a, these measurements are not new, but they were first presented in the PhD work [35]. Here the sensor atmosphere was subsequently cycled with equal time intervals of 100% air and 100% VOC. Here too, stress-related phenomena were not present in the measurements.

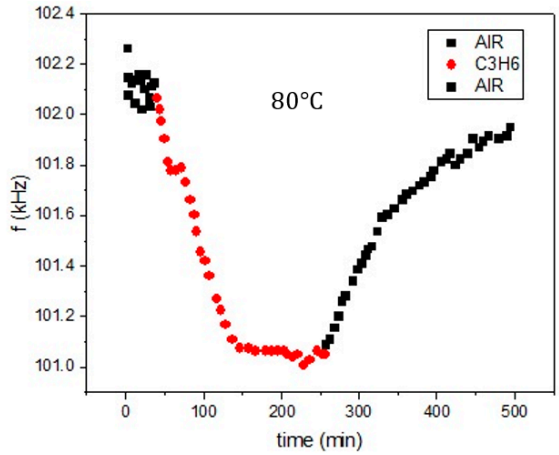

Figure 5. Data from PhD work [35], which corresponds to different propene concentrations on a Metglas/Linde Type A (LTA) sensor.

4. Discussion

As it was mentioned above, the main purpose of the current paper is to introduce a new method to extract the diffusion constant D of various VOC in Zeolites, given plots like the ones shown in Figures 4 and 5. Our proposed method, consists of the following steps:

- Assume the sensor geometry of Figure 6.
- Solve the differential Equation (2) by applying the appropriate boundary and initial conditions for the VOC concentration c.

- Extract an expression for the VOC adsorbed mass $\Delta m(t)$ in the Zeolite film versus time. This expression includes the diffusion constant D as a parameter.
- Substitute $\Delta m(t)$ in Equation (1) to extract a corresponding expression of the sensor resonance frequency f versus time.
- Fit the f expression found in the previous step to the data of Figures 4 and 5 with D as the running parameter and get its optimum value for best fit.

The math details and calculations of the proposed method are explained in detail in the Appendix A, Appendix B, Appendix C. It will only be mentioned here that the fit was applied to only one of the multiple branches of the plots of Figures 4 and 5 and, more specifically, to one of the diffusion-out branches, when the VOC flow at the sensor neighborhood is set to zero (leaving only a flow of synthetic air around the sensor which causes no adsorption according to Figure 2), as this process leads to an easy exponential solution of the differential Equation (2).

Additionally, the basic assumptions of the method need to be given here. As Figure 6 shows, our sensor consists of the zeolite adsorbing film on top of a Metglas strip. The film has the form of a thin slab so most of the gas escapes from the top surface and not sideways as the film thickness is about 30 μm, which is much smaller than the other two dimensions of 4 and 20 mm. Thus, the gas concentration in the film, will be considered to be constant over y and z (except only for a small fraction at the edges) and have a strong x profile along the film's thickness. That makes the problem one-dimensional which simplifies the whole analysis.

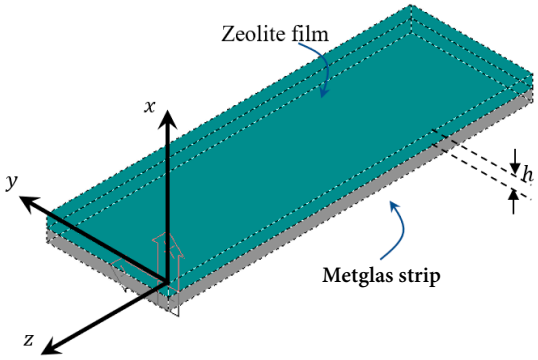

Figure 6. Sensor geometry.

The analysis in the Appendix B leads to the following Equation (A11) for the sensor resonance frequency f versus time

$$f \approx f_0\left[1 - \frac{4hc_0}{m\pi^2}\exp\left(-\frac{D\pi^2}{4h^2}t\right)\right] \tag{3}$$

where f_0 is the resonance frequency without mass load (basically with air flow as in Figure 2), h is the zeolite film thickness, c_0 is the initial VOC concentration in units g/μm inside the film (from the previous diffusion-in process, where c_0 is assumed to be constant over the film thickness), and m is the clear sensor mass without adsorption. Equation (3) is a simple exponential expression of the form $f = f_0\left(1 - ae^{-bt}\right)$ with

$$a = \frac{4hc_0}{m\pi^2} \tag{4}$$

and

$$b = \frac{D\pi^2}{4h^2} \tag{5}$$

so it can easily be fit to get a and b, in order to extract D from the simple expression

$$D = \frac{4h^2 b}{\pi^2} \tag{6}$$

Shown in Figures 7 and 8 are the fits of the plots of Figures 4 and 5, correspondingly, of only the first diffuse-out branch (the second marked "AIR" branch in the plots). The corresponding fit parameters and diffusion coefficients are shown in Table 2.

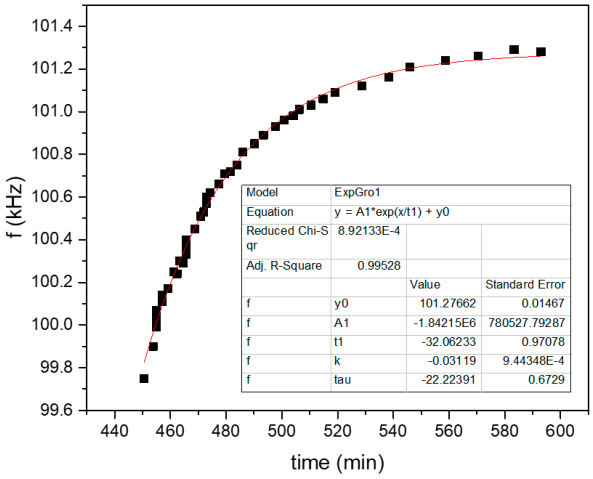

Figure 7. Exponential fit of the second branch marked "AIR" at the plot of Figure 4.

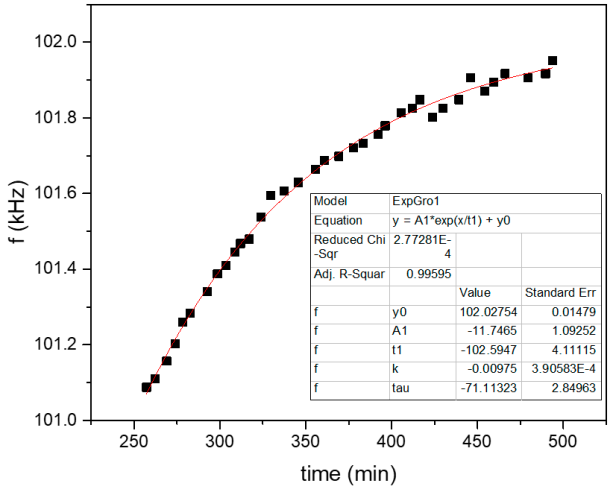

Figure 8. Exponential fit of the second branch marked "AIR" at the plot of Figure 5.

Table 2. Fit results of Figures 7 and 8.

	h (μm)	b (min^{-1})	D (m^2/s)	θ (°C)
FAU/p-Xylene	30	0.0312	1.89×10^{-13}	120
LTA/propene	30	0.00975	5.9×10^{-14}	80

Thus the mini review list of Table 1 in Section 1, can be enriched by adding two extra lines for the cases of p-Xylene in FAU type zeolite and propene in LTA type zeolite of the current work, with corresponding diffusion coefficients D of 1.89×10^{-13} m^2/s at 120 °C and 5.9×10^{-14} m^2/s at 80 °C, correspondingly. Both results are within the order of magnitude of the values presented in the table.

5. Conclusions

A new experimental technique was proposed which is able to determine the diffusion coefficient of a gas in a porous adsorbing medium such as a zeolite, but it can equally being applied to other porous materials. The technique is based on the use of resonance data from magnetoelastic sensors,

enhanced by an exponential data fit model of Fickian type diffusion. The method is demonstrated for two different cases, the adsorption of p-Xylene vapor in a FAU zeolite and propene gas in an LTA zeolite and the corresponding diffusion coefficients D of 1.89×10^{-13} m^2/s at 120 °C and 5.9×10^{-14} m^2/s at 80 °C, which are reported here for first time and are within the order of magnitude of results found for other pairs in the literature. The importance of the current work for future study is that more pairs of VOC/zeolite diffusion coefficients can be easily measured as there are not so many data available in the literature, thus enriching Table 1 and providing a good reference for research in the field.

Author Contributions: Conceptualization, D.K.; methodology, D.K., T.B. and G.S.; software, G.S.; validation, D.K. and G.S.; formal analysis, D.K. and T.B.; investigation, D.K. and T.B.; resources, G.S.; data curation, G.S.; visualization, T.B.; supervision, D.K.; project administration, D.K.; funding acquisition, G.S.; writing—original draft preparation, D.K.; writing—review and editing, D.K. and G.S. All authors have read and agreed to the published version of the manuscript.

Funding: The present work was partly supported by the Andreas Mentzelopoulos Scholarships for the University of Patras.

Conflicts of Interest: The authors declare no conflict of interest.

Appendix A. Mathematics of Diffusion

In what follows, we will follow the analysis in [36]. The basic equation that governs the diffusion process in one dimension is

$$\frac{\partial c}{\partial t} = D\frac{\partial^2 c}{\partial x^2} \tag{A1}$$

where c is the concentration of the adsorbed gas molecules (mass per distance for problems in one dimension) and D their diffusion coefficient in the host zeolite. As shown in Figure A1 below, our zeolite film of thickens h is confined between the plane $x = 0$, which is the zeolite-sensor interface, and $x = h$ which is the open surface. The other two film dimensions y and z are considered to be infinite. It is assumed that the film was exposed for long time to a steady gas flow which brings the film to a saturated state with a constant concentration $c = c_0$ all over the film. That will be the initial condition at $t = 0$. Then, suddenly, the gas flow is interrupted, and the gas is slowly diffusing out from the free end at $x = h$ where the concentration is considered to be zero, which means $c(h, t) = 0$ for all times $t > 0$. As the diffusion progresses, a certain amount of gas is still present in the film and we would like to know the concentration profile so as to calculate the remaining gas mass. Another boundary condition is at the $x = 0$ surface where the gas cannot escape out and thus its flow there is zero. This mathematically is expressed by a flat curve at this edge, in other words $\partial c(0, t)/\partial x = 0$ for all times $t > 0$. We expect the concentration to have a general form like the one shown with a blue dashed line in the figure.

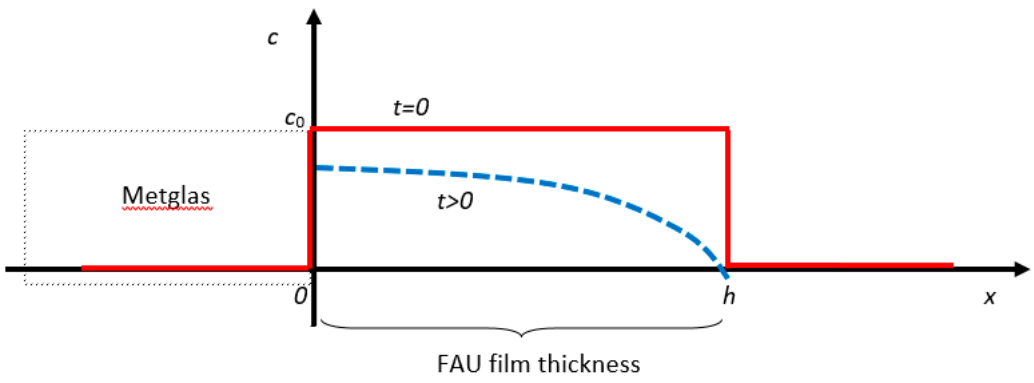

Figure A1. Initial and later gas concentration across the film thickness.

In Section 2.3 of [36], the author gives a general solution of the diffusion Equation (A1) by the method of separation of variables. The solution has the form (Equation 2.24 in the Reference [36])

$$c = (A \sin \lambda x + B \cos \lambda x) \exp\left(-D\lambda^2 t\right) \tag{A2}$$

From the second boundary condition $\partial c(0,t)/\partial x = 0$, we have necessarily $A = 0$. From the other boundary condition $c(h,t) = 0$, we have

$$\cos \lambda h = 0 => \lambda h = (2n+1)\frac{\pi}{2}$$

or

$$\lambda_n = (2n+1)\frac{\pi}{2h} \tag{A3}$$

where $n = 0, 1, 2, \ldots$. Since for each n we have a different solution in Equation (A2), the most general solution is the sum of all solutions (because the differential Equation (A1) is linear in c). Summing all terms, we get

$$c(x,t) = \sum_{n=0}^{\infty} B_n \cos(\lambda_n x) \exp\left[-D{\lambda_n}^2 t\right] \tag{A4}$$

where λ_n is given by Equation (A3). From the initial condition at $t = 0$ we have for each x in the film

$$c_0 = \sum_{n=0}^{\infty} B_n \cos(\lambda_n x) \tag{A5}$$

We can use this relationship to find B_n with the help of the cosine orthogonality rule according to which:

$$\int_0^h \cos \lambda_n x \cos \lambda_m x dx = \frac{h}{2}\delta_{mn} \tag{A6}$$

To make use of this rule, we multiply Equation (5) by $\cos(\lambda_m x)$ and integrate from $x = 0$ to $x = h$:

$$\int_0^h c_0 \cos(\lambda_m x) dx = \sum_{n=0}^{\infty} B_n \int_0^h \cos(\lambda_m x) \cos(\lambda_n x) dx$$

or

$$c_0 \frac{\sin(\lambda_m h)}{\lambda_m} = \frac{h}{2} \sum_{n=0}^{\infty} B_n \delta_{mn} => \frac{c_0}{\lambda_m} \sin\left[(2m+1)\frac{\pi}{2}\right] = \frac{h}{2} B_m$$

In the last step, use was made of Equations (A3) and (A6). The sine term evaluates at even multiples of $\pi/2$ so it is either 1 or -1, depending on the value of m. Therefore,

$$B_m = \frac{2c_0}{h\lambda_m}(-1)^m = \frac{4c_0}{(2m+1)\pi}(-1)^m$$

Equation (A4) then becomes

$$c = \sum_{n=0}^{\infty} \frac{4c_0}{(2n+1)\pi}(-1)^n \exp\left[-D{\lambda_n}^2 t\right] \cos(\lambda_n x) \tag{A7}$$

For increasing values of n, the factor $(2n+1)^2$ becomes increasingly larger, like 1, 9, 25, 49, ... etc., and it appears both in the denominator and the exponent of each term in the sum. Thus, successive terms in the sum are by far smaller than the previous terms. That means that it is a good approximation to keep only the $n = 0$ term in Equation (A7) and have

$$c = \frac{4}{\pi} c_0 \exp\left[-D{\lambda_0}^2 t\right] \cos(\lambda_0 x) \tag{A8}$$

where $\lambda_0 = \pi/2h$ (Equation (A4)). To find the total mass $\Delta m(t)$ that remains in the film at time t (part of the mass diffuses out of the film), we need to integrate Equation (A8) from $x = 0$ to $x = h$. Since

$$\int_0^h \cos(\lambda_0 x) dx = \frac{\sin(\lambda_0 h)}{\lambda_0} = \frac{2h}{\pi} \sin\frac{\pi}{2} = \frac{2h}{\pi}$$

we have

$$\Delta m(t) = \int_o^h c dx = \frac{8h}{\pi^2} c_0 \exp\left[-D{\lambda_0}^2 t\right]$$

The limiting values of the mass are $\Delta m(\infty) \to 0$ for $t \to \infty$ as expected, and the initial value

$$\Delta m(0) = \frac{8h}{\pi^2} c_0$$

for $t = 0$.

Appendix B. Connection with the Resonance Frequency

The density ρ of the sensor when no gas is present is $\rho = m/V$ which changes under adsorption to:

$$\rho = \frac{m + \Delta m}{V} \tag{A9}$$

where m is the sensor's mass in vacuum (with no adsorption), V its volume, and Δm the amount of the adsorbed mass. From Equation (1) in the main context of the current paper, we have:

$$f = \frac{1}{2L} \sqrt{\frac{E}{\rho}}$$

where E is the sensor Young's modulus and L its length. With the help of Equation (A9) this becomes

$$f = \frac{1}{2L} \sqrt{\frac{VE}{m + \Delta m}} \tag{A10}$$

Typically, the mass load Δm is but a tiny percent of the total mass m of the sensor which means that $\Delta m/m \ll 1$. Using the approximation $(1 + x)^n \approx 1 + nx$ for small x, we have

$$f = \frac{1}{2L} \sqrt{\frac{VE}{m + \Delta m}} = \frac{1}{2L} \sqrt{\frac{VE}{m(1 + \Delta m/m)}} \approx f_0 \left(1 - \frac{1}{2} \frac{\Delta m}{m}\right)$$

where f_0 is the resonance frequency without mass load (the f of Equation (A10) for $\Delta m = 0$). With the help of Equation (A9) the above expression becomes:

$$f \approx f_0 \left[1 - \frac{4h}{m\pi^2} c_0 \exp\left(-\frac{D\pi^2}{4h^2} t\right)\right] \tag{A11}$$

where the value $\lambda_0 = \pi/2h$ from Equation (3) was used in the exponent. The above equation has a simple exponential form

$$f = f_0 \left(1 - ae^{-bt}\right)$$

where

$$a = \frac{4hc_0}{m\pi^2} \tag{A12}$$

and

$$b = \frac{D\pi^2}{4h^2} \tag{A13}$$

Appendix C. Orthogonality Condition

Proof of orthogonality of $\cos \lambda_n x$ functions: from basic trigonometry we have

$$2 \cos \lambda_n x \ \cos \lambda_m x = \cos(\lambda_n + \lambda_m)x + \cos(\lambda_n - \lambda_m)x$$

Consider two different cases:
(a) Case $m \neq n$

$$\begin{aligned} 2\int_0^h \cos \lambda_n x \cos \lambda_m x dx &= \int_0^h \cos(\lambda_n + \lambda_m)x dx + \int_0^h \cos(\lambda_n - \lambda_m)dx \\ &= \tfrac{1}{(\lambda_n+\lambda_m)}[\sin(\lambda_n + \lambda_m)x]_0^h + \tfrac{1}{(\lambda_n-\lambda_m)}[\sin(\lambda_n - \lambda_m)x]_0^h \\ &= \tfrac{1}{(\lambda_n+\lambda_m)} \sin(\lambda_n + \lambda_m)h + \tfrac{1}{(\lambda_n-\lambda_m)} \sin(\lambda_n - \lambda_m)h \\ &= \tfrac{1}{(\lambda_n+\lambda_m)} \sin(2n + 2m + 2)\tfrac{\pi}{2} + \tfrac{1}{(\lambda_n-\lambda_m)} \sin(2n - 2m)\tfrac{\pi}{2} \end{aligned}$$

In both expressions, the argument of the sine function is an even integer times $\pi/2$ which evaluates to either π or 2π (in the first trigonometric cycle) where the sine is zero. Therefore, when n differs from m we have:

$$\int_0^h \cos \lambda_n x \cos \lambda_m x dx = 0$$

(b) Case $m = n$
We have

$$\begin{aligned} 2\int_0^h \cos \lambda_n x \cos \lambda_n x dx &= \int_0^h \cos(2\lambda_n)x dx + \int_0^h \cos(0)dx \\ &= \tfrac{1}{2\lambda_n}[\sin(2\lambda_n)x]_0^h + \int_0^h dx = \tfrac{1}{2\lambda_n} \sin(2\lambda_n h) + h \\ &= \tfrac{1}{2\lambda_n} \sin(2n + 1)\pi + h = h \end{aligned}$$

Concluding the two cases, we can write this in one formula:

$$\int_0^h \cos \lambda_n x \cos \lambda_m x dx = \frac{h}{2}\delta_{mn}$$

References

1. Ren, L.; Yu, K.; Tan, Y. Applications and advances of magnetoelastic sensors in biomedical engineering: A review. *Materials* **2019**, *12*, 1135. [CrossRef] [PubMed]
2. Beltrami, L.V.R.; Beltrami, M.; Roesch-Ely, M.; Kunst, S.R.; Missell, F.P.; Birriel, E.J.; de FMalfatti, C. Magnetoelastic sensors with hybrid films for bacteria detection in milk. *J. Food Eng.* **2017**, *212*, 18–28. [CrossRef]
3. Jiang, Q.; Chen, P.; Li, S.; Zhao, H.; Liu, Y.; Horikawa, S.; Chin, B.A. A highly integratable microfluidic biosensing chip based on magnetoelastic-sensor and planar coil. In Proceedings of the 2016 IEEE SENSORS, Orlando, FL, USA, 30 October–3 November 2016. [CrossRef]
4. Chen, I.H.; Horikawa, S.; Bryant, K.; Riggs, R.; Chin, B.A.; Barbaree, J.M. Bacterial assessment of phage magnetoelastic sensors for salmonella enterica typhimurium detection in chicken meat. *Food Control* **2017**, *71*, 273–278. [CrossRef]
5. Samourgkanidis, G.; Nikolaou, P.; Gkovosdis-Louvaris, A.; Sakellis, E.; Blana, I.M.; Topoglidis, E. Hemin-Modified SnO_2/Metglas Electrodes for the Simultaneous Electrochemical and Magnetoelastic Sensing of H_2O_2. *Coatings* **2018**, *8*, 284. [CrossRef]

6. Baimpos, T.; Tsukala, V.; Nikolakis, V.; Kouzoudis, D. A modified method for the calculation of the humidity adsorption stresses inside zeolite films using magnetoelastic sensors. *Sens. Lett.* **2012**, *10*, 879–885. [CrossRef]
7. Landau, L.D.; Lifshitz, E.M. *Theory of Elasticity*, 3rd ed.; Pergamon: Oxford, UK, 1986.
8. Baimpos, T.; Gora, L.; Nikolakis, V.; Kouzoudis, D. Selective detection of hazardous VOC using zeolite/Metglas composite sensors. *Sens. Actuators A* **2012**, *186*, 21–31. [CrossRef]
9. Ju, J.F.; Syu, M.J.; Teng, H.S.; Chou, S.K.; Chang, Y.S. Preparation and identification of β-cyclodextrin polymer thin film for quartz crystal microbalance sensing of benzene, toluene, and p-Xylene. *Sens. Actuators B* **2008**, *132*, 319. [CrossRef]
10. Matsuguchi, M.; Uno, T.; Aoki, T.; Yoshida, M. Chemically modified copolymer coatings for mass-sensitive toluene vapor sensors. *Sens. Actuators B* **2008**, *131*, 652. [CrossRef]
11. Dermody, D.; Crooks, R.; Kim, T. Interactions between Organized, Surface-Confined Monolayers and Vapor-Phase Probe Molecules. 11. Synthesis, Characterization, and Chemical Sensitivity of Self-Assembled Polydiacetylene/Calixn.arene Bilayers. *J. Am. Chem. Soc.* **1996**, *118*, 11912. [CrossRef]
12. Lange, D.; Hagleitner, C.; Hierlemann, A.; Brand, O.; Baltes, H. Complementary metal oxide semiconductor cantilever arrays on a single chip: Mass-sensitive detection of volatile organic compounds. *Anal. Chem.* **2002**, *74*, 3084. [CrossRef]
13. Kozlowski, M.; Diduszko, R.; Olszewska, K.; Wronka, H.; Czerwosz, E. Nanostructural palladium films for sensor applications. *Vacuum* **2008**, *82*, 956. [CrossRef]
14. Penza, M.; Cassano, G.; Aversa, P.; Cusano, A.; Cutolo, A.; Giordano, M.; Nicolais, L. Carbon nanotube acoustic and optical sensors for volatile organic compound detection. *Nanotechnology* **2005**, *16*, 2536. [CrossRef]
15. Raso, R.A.; Stoessel, P.R.; Stark, W.J. Physical mixtures of CeO_2 and zeolites as regenerable indoor air purifiers: Adsorption and temperature dependent oxidation of VOC. *J. Mater. Chem. A* **2014**, *2*, 14089–14098. [CrossRef]
16. Izadyar, S.; Fatemi, S. Fabrication of X Zeolite Based Modified Nano TiO_2 Photocatalytic Paper for Removal of VOC Pollutants under Visible Light. *Ind. Eng. Chem. Res.* **2013**, *52*, 10961–10968. [CrossRef]
17. Biomorgi, J.; Haddou, M.; Oliveros, E.; Maurette, M.T.; Benoit-Marquié, F. Coupling of adsorption on zeolite and V-UV irradiation for the treatment of VOC containing air streams: Effect of TiO_2 on the VOC degradation efficiency. *J. Adv. Oxid. Technol.* **2010**, *13*, 107–115. [CrossRef]
18. Nikolajsen, K.; Kiwi-Minsker, L.; Renken, A. Structured fixed-bed adsorber based on zeolite/sintered metal fibre for low concentration VOC removal. *Chem. Eng. Res. Des.* **2006**, *84*, 562–568. [CrossRef]
19. Sutradhar, M.; Barman, T.R.; Alegria, E.C.; da Silva, M.F.C.G.; Liu, C.M.; Kou, H.Z.; Pombeiro, A.J. Cu(ii) complexes of N-rich aroylhydrazone: Magnetism and catalytic activity towards microwave-assisted oxidation of xylenes. *Dalton Trans.* **2019**, *48*, 12839–12849. [CrossRef]
20. Sutradhar, M.; Barman, T.R.; Alegria, E.C.B.A.; Lapa, H.M.; da Silva, M.F.C.G.; Pombeiro, A.J.L. Cd(ii) coordination compounds as heterogeneous catalysts for microwave-assisted peroxidative oxidation of toluene and 1-phenylethanol. *New J. Chem.* **2020**. [CrossRef]
21. Sutradhar, M.; Alegria, E.C.; Barman, T.R.; Scorcellettia, F.; da Silva, M.F.; Pombeiro, A.J. Microwave-assisted peroxidative oxidation of toluene and 1-phenylethanol with monomeric keto and polymeric enol aroylhydrazone Cu(II) complexes. *Mol. Cat.* **2017**, *439*, 224–232. [CrossRef]
22. Karger, J.; Vasenkov, S. Quantitation of diffusion in zeolite catalysts. *Microporous Mesoporous Mater.* **2005**, *85*, 195–206. [CrossRef]
23. Baimpos, T.; Kouzoudis, D.; Gora, L.; Nikolakis, V. Are zeolite films flexible? *Chem. Mater.* **2011**, *23*, 1347–1349. [CrossRef]
24. Krishna, R. Diffusing uphill with James Clerk Maxwell and Josef Stefan. *Rev. Pap. Chem. Eng. Sci.* **2019**, *195*, 851–880. [CrossRef]
25. Masuda, T.; Hashimoto, H. Measurements of Adsorption on Outer Surface of Zeolite and their Influence on Evaluation of Intracrystalline Diffusivity. In Proceedings of the International Symposium on Zeolites and Microporous Systems, Nagoya, Japan, 22–25 August 1993; Volume 83, p. 225.
26. Xiao, J. The Diffusion Mechanism of Hydrocarbons in Zeolites. Ph.D. Thesis, Massachusetts Institute of Technology, Cambridge, MA, USA, April 1990; p. 108.
27. Auerbach, S.M.; Carrado, K.A.; Dutta, P.K. (Eds.) *Handbook of Zeolite Science and Technology*, 1st ed.; CRC Press: Boca Raton, FL, USA, 31 July 2003; ISBN 9780824740207.

28. Danny, S. Diffusion in Zeolites: Towards a Microscopic Understanding. Ph.D. Thesis, Eindhoven University of Technology, Eindhoven, The Netherlands, 2002.
29. Möller, A.; Guimaraes, A.P.; Gläser, R.; Staudt, R. Uptake-curves for the determination of diffusion coefficients and sorption equilibria for n-alkanes on zeolites. *Microporous Mesoporous Mater.* **2009**, *125*, 23–29. [CrossRef]
30. Koriabkina, A.O. Diffusion of Alkanes in MFI-type Zeolites. Ph.D. Thesis, Technische Universiteit Eindhoven, Eindhoven, The Netherlands, 2003. [CrossRef]
31. Brandani, S.; Xu, Z.; Ruthven, D. Transport diffusion and self-diffusion of benzene in NaX zeolite crystals studied by ZLC and tracer ZLC methods. *Microporous Mater.* **1996**, *7*, 323–331. [CrossRef]
32. Gautam, S.; Tripathi, A.K.; Kamble, V.S.; Mitra, S.; Mukhopadhyay, R. Diffusion of propylene adsorbed in Na-Y and Na-ZSM5 zeolites: Neutron scattering and FTIR studies. *Pramana J. Phys.* **2008**, *71*, 1153–1157. [CrossRef]
33. Gonsalves, J.A.S.; Portsmouth, R.L.; Alexander, P.; Gladden, L.F. Intercage and Intracage Transport of Aromatics in Zeolites NaY, HY, and USY Studied by 2H NMR. *J. Phys. Chem.* **1995**, *99*, 3317–3325. [CrossRef]
34. Donk, S.V. Adsorption, Diffusion and Reaction Studies of Hydrocarbons on Zeolite Catalysts. Ph.D. Thesis, Utrecht University, Utrecht, Holland, 2002.
35. Baimpos, T. Composition of zeolite membranes on the surface of magnetoelastic sheets to detect volatile organic substances and determine the effect of drinking on the mechanical properties of the film. Ph.D. Thesis, University of Patras, Patras, Greece, 2012. Available online: http://hdl.handle.net/10889/5506 (accessed on 6 June 2020). (In Greek).
36. Crank, J. *The Mathematics of Diffusion*, 2nd ed.; Clarendon Press: Oxford, UK, 1975.